Rovibronic bands of the A X transition of C H 3 O O and C D 3 O O detected with cavity ringdown absorption near 1.2 – 1.4 m

Chao-Yu Chung, Chi-Wen Cheng, Yuan-Pern Lee, Hsin-Yi Liao, Erin N. Sharp, Patrick Rupper, and Terry A. Miller

Citation: The Journal of Chemical Physics **127**, 044311 (2007); doi: 10.1063/1.2747616
View online: http://dx.doi.org/10.1063/1.2747616
View Table of Contents: http://scitation.aip.org/content/aip/journal/jcp/127/4?ver=pdfcov
Published by the AIP Publishing

Rovibronic bands of the $\tilde{A}\leftarrow\tilde{X}$ transition of CH_3OO and CD_3OO detected with cavity ringdown absorption near 1.2–1.4 μm

Chao-Yu Chung, Chi-Wen Cheng, and Yuan-Pern Lee[a),b)]
Department of Applied Chemistry, National Chiao Tung University, 1001, Ta-Hsueh Road, Hsinchu 30010, Taiwan; Institute of Molecular Science, National Chiao Tung University, 1001, Ta-Hsueh Road, Hsinchu 30010, Taiwan; and Institute of Atomic and Molecular Sciences, Academia Sinica, Taipei 10617, Taiwan

Hsin-Yi Liao
Department of Science Education, National Taipei University of Education, 134, Section 2, Heping E. Road, Da-an District, Taipei 10659, Taiwan

Erin N. Sharp, Patrick Rupper, and Terry A. Miller[a),c)]
Laser Spectroscopy Facility, Department of Chemistry, The Ohio State University, 120 W. 18th Avenue, Columbus, Ohio 43210

(Received 3 April 2007; accepted 15 May 2007; published online 27 July 2007)

We have recorded several rovibronic bands of CH_3OO and CD_3OO in their $\tilde{A}\leftarrow\tilde{X}$ transitions in the range of 1.18–1.40 μm with the cavity ringdown technique. While the electronic origins for these species have been reported previously, many newly observed rovibronic bands are described here. The experimental vibrational frequencies (given as ν in the unit cm^{-1} in this paper) for the COO bending (ν_8) and COO symmetric stretching (ν_7) modes in the $\tilde{A}$ state are 378 and 887 cm^{-1} for CH_3OO, and 348 and 824 cm^{-1} for CD_3OO, respectively. In addition, two other vibrational frequencies were observed for the $\tilde{A}$ state of CD_3OO, namely, ν_5 (954 cm^{-1}) and ν_6 (971 cm^{-1}). These experimental vibrational frequencies for the $\tilde{A}$ state of both CH_3OO and CD_3OO are in good agreement with predictions from quantum-chemical calculations at the UB3LYP/aug-cc-pVTZ level. The enhanced activity of the ν_5 vibrational mode in CD_3OO is rationalized by mode mixing with the ν_7 mode, as supported by calculations of multidimensional Franck-Condon factors. In addition, many hot bands involving the methyl torsional mode (ν_{12}) are observed for both normal and deuterated methyl peroxy. These bands include the "typical" sequence transitions and some "atypical" ones due to the nature of the eigenvalues and eigenfunctions which are a consequence of the low, but very different, torsional barriers in the $\tilde{X}$ and $\tilde{A}$ states. In addition, the 12_2^2 band in CH_3OO and the 12_3^3 band in CD_3OO show quite different structures than the origin bands, an effect which results from tunneling splittings comparable to the rotational contour. © *2007 American Institute of Physics*. [DOI: 10.1063/1.2747616]

I. INTRODUCTION

Alkyl peroxy radicals are important intermediates in the oxidation of organic compounds, both in the atmosphere[1,2] and under combustion conditions.[3] These alkyl peroxy radicals are typically formed via termolecular reactions between alkyl radicals, O_2, and a third body. Reactions of alkyl peroxy radicals with NO produce NO_2, which leads to the formation of ozone in the troposphere. Self-reactions and the reaction of alkyl peroxy radicals with HO_2 are also important in the HO_x catalytic cycle of the atmosphere.[4]

Methyl peroxy (CH_3OO), the simplest alkyl peroxy radical, has a ground electronic state designated as $\tilde{X}\,^2A''$. Although 10 of the 12 fundamental vibrational modes were identified for matrix-isolated CH_3OO,[5,6] the infrared (IR) spectrum of gaseous CH_3OO is still unreported. Previous detection and kinetic investigations of gaseous CH_3OO utilized the intense UV absorption of the $\tilde{B}\,^2A''\leftarrow\tilde{X}\,^2A''$ transition near 240 nm,[7] but the broad and unstructured nature of this system precludes analysis of its vibrational or rotational structure; selective detection among various alkyl peroxy radicals using this electronic transition is unlikely.

The weak $\tilde{A}\,^2A'\leftarrow\tilde{X}\,^2A''$ system of CH_3OO was initially reported by Hunziker and Wendt, who applied modulated Hg-photosensitized decomposition of a mixture containing acetone, O_2, and N_2 to produce CH_3OO, and detected it through phase-sensitive absorption.[8] They reported that this $\tilde{A}\leftarrow\tilde{X}$ system consisted mainly of an intense origin at a frequency of 7375 cm^{-1} (here and throughout the paper we report frequencies in units of cm^{-1} which must be multiplied by the speed of light to yield values in Hz) and two weak bands at 8271 and 9149 cm^{-1}; the progression with spacings of about 896 cm^{-1} was assigned to the O–O stretching mode of CH_3OO. Pushkarsky *et al.* photolyzed, with an excimer laser at either 193 or 248 nm, a flowing mixture containing

[a)]Authors to whom correspondence should be addressed.
[b)]Electronic mail: yplee@mail.nctu.edu.tw
[c)]Electronic mail: tamiller@chemistry.ohio-state.edu

Ne, O_2, and a precursor of CH_3 (either acetone or methyl iodide) or its perdeuterated variant to produce CH_3OO or CD_3OO.[9] They employed the cavity ringdown technique to detect the origin bands of the $\tilde{A} \leftarrow \tilde{X}$ system near 1.35 μm and reported $\nu_0 = 7382.8 \pm 0.5$ cm^{-1} for CH_3OO and 7372.6 ± 0.5 cm^{-1} for CD_3OO; rotational parameters of the lower and upper states were also fitted. They also detected a weaker band ~ 100 cm^{-1} above the origin and tentatively assigned it as a hot band initiated from the $\nu_{12}=1$ level of the CH_3 torsional mode, as Hunziker and Wendt proposed.[8] This sensitive detection technique was later employed to investigate kinetics involving CH_3OO.[10] Blanksby *et al.* employed photodetachment to record the photoelectron spectrum of CH_3OO^- and reported the origin[11] of the $\tilde{A} \leftarrow \tilde{X}$ transition of CH_3OO to be 7372 ± 40 cm^{-1}, consistent with previous reports.[8,9] Fu *et al.* recently employed IR and vacuum ultraviolet (vuv) lasers to record photofragmentation detection (PFD) spectra of CH_3OO and CD_3OO and reported $\nu_6 = 1002$ cm^{-1} and $\nu_7 = 898$ cm^{-1} for CH_3OO, and $\nu_3 - \nu_7 = 986$, 1056, 899, 963, and 834 cm^{-1} for CD_3OO.[12]

Endo and co-workers recently evaluated the rotational parameters of CH_3OO with Fourier transform microwave spectroscopy;[13] their results deviate from those reported by Pushkarsky *et al.*[9] within 1% of the A value and 6% of the B and C values for CH_3OO in its $\tilde{X}\,^2A''$ state.

The geometry and vibrational frequencies of the ground electronic state have been investigated quantum chemically using various methods.[6,14–17] The first electronic excited state $\tilde{A}\,^2A'$ was predicted to lie at 7267–9656 cm^{-1} above the ground state, depending on the method used.[16,17] Fu *et al.*[12] employed the B3LYP/aug-cc-pVDZ method and predicted vibrational frequencies of the $\tilde{A}$ state.

We have employed the cavity ringdown technique near the 1.2–1.4 μm region to investigate rovibronic bands of gaseous CH_3OO and CD_3OO in their $\tilde{A} \leftarrow \tilde{X}$ transitions. Many vibronic bands were observed, and several vibrational frequencies of the $\tilde{A}$ state were experimentally determined for the first time.

II. EXPERIMENTS

The basic principles and experiments of cavity ringdown have been discussed extensively.[18] For absorption spectra based on cavity ringdown one measures the decay of intensity of a laser pulse trapped in an optical cavity formed between two highly reflective mirrors. When the cavity contains an absorbing medium, which for these experiments is CH_3OO or CD_3OO, the ringdown period is decreased at those wavelengths at which absorption occurs. In the equation

$$I = I_0 e^{-ct(1-R+\alpha l)/L}, \tag{1}$$

I_0 and I are the intensities of incident and transmitted light, respectively, c is the speed of light, t is time, R is the reflectivity of the mirror, l is the path length of the absorbing medium, L is the length of the cavity, and $\alpha = \sigma N$ is the absorption coefficient, where σ is the cross section of absorption and N is the number density of absorbing molecules. The pertinent quantity for cavity ringdown spectroscopy is the absorption αl of a sample per pass through the cavity.

The ringdown period τ is defined as the temporal interval required for the intensity to decay to $1/e$ of its initial value. When there is no absorption, as in the absence of a sample, the ringdown period is

$$\tau = L/[c(1-R)], \tag{2}$$

whereas in the presence of an absorbing species at a particular wavelength the ringdown period becomes

$$\tau' = L/[c(1-R+\alpha l)]. \tag{3}$$

The absorption per unit length is hence simply related to the cavity ringdown periods as follows:

$$\alpha = \left(\frac{1}{\tau'} - \frac{1}{\tau}\right)\frac{L}{cl}. \tag{4}$$

There were two different experimental setups utilized to collect the data presented in this paper. The data in the 7200–8200 cm^{-1} region were collected at Ohio State University, where the cavity ringdown apparatus was similar to that used in previous studies of the $\tilde{A} \leftarrow \tilde{X}$ transition of other alkyl peroxy radicals by Miller and co-workers,[19,20] and therefore only a brief description is given here. IR radiation in the region of 1.22–1.39 μm was generated by Raman shifting the output of a dye laser in molecular hydrogen. A Nd:YAG (yttrium aluminum garnet) pumped dye laser system (PRO-270, Spectra Physics; Sirah) operating at 20 Hz produced 50–100 mJ/pulse of tunable radiation in the region of 605–644 nm with 4-dicyanomethylene-2-methyl-6-*p*-dimethylaminostyryl-4*H*-pyran (DCM), Rhodamine B, and Rhodamine 101 laser dyes. The output of the dye laser was focused into a 70 cm long single-pass Raman cell filled with 17–24 bars of gaseous H_2. The output radiation from the Raman cell was spectrally filtered to eliminate visible anti-Stokes, and first Stokes components in order to only transmit second Stokes light. The resulting second Stokes radiation of 1–2 mJ was then directed into the cavity ringdown cell to probe the desired electronic transition in the peroxy radicals. The ringdown cavity, fabricated of stainless steel, consists of a 20 cm central part with two rectangular UV grade quartz photolysis windows and two arms of 15 cm in length each. The cavity ringdown mirrors (Los Gatos Research) were positioned at the ends of the arms on adjustable mounts. An InGaAs (PDA400, Thorlabs) photodiode was used to detect the outcoming radiation, and its output was recorded by a 12 bit digitizing card (Measurement Computing) for further analysis.

An excimer laser (LPX120icc, Lambda Physik) was used to photolyze acetone and d_6-acetone at 193 nm to produce CH_3 and CD_3 radicals, respectively. The photolysis beam was shaped by cylindrical and spherical lenses to form a rectangle (0.5×13 cm) and sent through the quartz windows into the central part of the flow cell. After CH_3/CD_3 radicals were produced by photolysis, they then reacted with molecular oxygen to form the desired CH_3OO/CD_3OO radicals. Typically, the ringdown cell was filled with a gas

mixture of 60 Torr O_2, 90 Torr N_2, and ~2–3 Torr acetone (or d_6-acetone). The photolysis pulse was fired approximately 100 μs before the dye laser, allowing enough time for the peroxy radicals to form, but not too much time to allow for radical-radical recombination or other secondary reactions. Background absorptions of the precursors and residual water vapor were eliminated by the subtraction of data points taken with the excimer laser on and off for each laser step. Our near infrared Raman-shifted frequencies were calibrated using the HITRAN (Ref. 21) database for water absorptions.

The data in the 8200–8600 cm^{-1} region were collected at National Chiao Tung University.[22] The laser radiation near 1.2 μm was generated with a single-pass Raman shifter employing gaseous H_2 at ~15 bars pumped with a dye laser (Spectra Physics, PDL-3, with a mixture of Exciton dyes LDS 821 and LDS 765), which is in turn pumped with a Nd:YAG laser (Spectra Physics, Lab 170, 30 Hz); output of the dye laser near 810 nm is ~30 mJ and that of the Raman-shifted beam near 1.2 μm is ~1 mJ. The spectral width of this laser system is ~0.13 cm^{-1} and the wavelength scanning steps were 0.01 nm (~0.1 cm^{-1}). We calibrated the wavelength of the dye laser with a wavemeter (Burleigh, WA4500) and lines of the $\tilde{a}\,^1\Delta_g\leftarrow\tilde{X}\,^3\Sigma_g^-$ system of molecular oxygen according to the HITRAN database.[21] The accuracy of measurements of wavelength is estimated to be ±0.012 nm. The ringdown signal was recorded with an InSb detector (Kolmar) cooled to 77 K. The signal was connected to a digital computer oscilloscope (14 bits, Gage Applied Technologies, Compuscope 14100), and subsequently processed with a personal computer. Typically the wave form was averaged over 60 laser pulses at each wavelength. The flow reactor, with physical length of 19.8 cm, has two rectangular (2.5×15 cm) photolysis ports on the side and was sealed with two quartz (S1UV) plates. The length of the cavity, formed between two highly reflective mirrors (Los Gatos Research, $R\cong0.9999$ near 1.2 μm), is 63 cm. The mirrors were purged with N_2 to avoid possible damage by the reactants. The total pressure of the system was typically 90 Torr with CH_3 precursor: $O_2:N_2\cong3:100:200$; CH_3 was produced by photolysis of acetone (Merck, HPLC grade) at 193 nm or CH_3I (Merck, 99%) at 248 nm (LPX110i, Lambda Physik, 30 Hz, 100 mJ at 193 nm and 240 mJ at 248 nm). The laser beam was expanded with a combination of a cylindrical lens and a spherical lens to have dimensions ~0.5×12 cm.

III. THEORETICAL CALCULATIONS

The geometries and vibrational frequencies of CH_3OO in its electronic ground and first excited states were optimized using the unrestricted hybrid density functional method with UB3LYP, Becke's three-parameter nonlocal-exchange functional and the nonlocal correlation functional of Lee, Yang, and Parr,[23,24] with various basis sets: 6-311G(d,p), 6-311++G($3df,3pd$), and aug-cc-pVTZ.[25,26] Zero-point energy (ZPE) corrections were included in adiabatic excitation energies using unscaled vibrational frequencies. All unrestricted density-functional theory calculations were performed with the GAUSSIAN 03 package.[27]

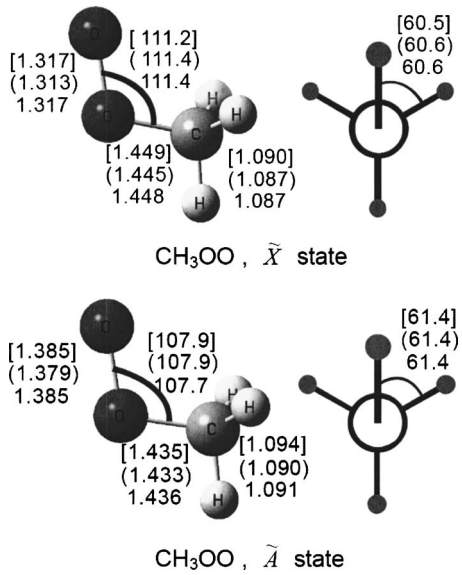

FIG. 1. UB3LYP optimized geometries (in Å and deg) for CH_3OO in its $\tilde{X}$ and $\tilde{A}$ states using various basis sets; bottom: aug-cc-pVTZ, parentheses: 6-311++G($3df,3pd$), square brackets: 6-311G(d,p).

For CH_3OO the ground state is $\tilde{X}\,^2A''$ and the first electronic excited state is $\tilde{A}\,^2A'$. The transition $\tilde{A}\leftarrow\tilde{X}$ involves excitation of an electron from the highest occupied molecular orbital (HOMO) to the singly occupied molecular orbital (SOMO). The HOMO appears to be σ^* along the C–O bond and nonbonding on the oxygen atoms on the molecular plane, whereas the SOMO has π^* character for the O–O bond.[17]

Figure 1 shows the structures of the CH_3OO radical in its ground and excited states, optimized using various basis sets. Predicted geometries show little dependence on the size of the basis sets employed; the bond lengths and angles of the ground state are similar to values previously reported using various methods.[12,14,15] Geometries of CD_3OO are nearly identical to those of CH_3OO. Excitation from the $\tilde{X}$ state to the $\tilde{A}$ state extends the O–O bond substantially, from 1.317 to 1.385 Å, and contracts the C–O bond slightly, from 1.448 to 1.436 Å; the angle ∠COO decreases from 111.4° to 107.7°. The change in lengths of the O–O and C–O bonds is consistent with characteristics associated with excitation of an electron from HOMO to SOMO.

Rotational parameters for CH_3OO and CD_3OO in their $\tilde{X}$ and $\tilde{A}$ states predicted with the UB3LYP/aug-cc-pVTZ calculations and those derived from experiments[9,13] are listed in Table I for comparison. Rotational parameters vary only slightly when the size of the basis set is varied.

Unscaled harmonic vibrational frequencies of CH_3OO and CD_3OO in their $\tilde{X}$ and $\tilde{A}$ states predicted with the UB3LYP method also show little effect on the size of the basis sets employed. Results for the $\tilde{X}$ and $\tilde{A}$ states predicted with UB3LYP/aug-cc-pVTZ are listed in Tables II and III, respectively, using the notation of Herzberg;[28] these frequencies are similar to those reported previously using B3LYP/aug-cc-pVDZ.[12] Approximate descriptions of these vibrational modes are also listed. The order of the frequency

TABLE I. Comparison of experimental and calculated rotational parameters A, B, and C (in cm^{-1}) of the $\tilde{X}$ and $\tilde{A}$ states of CH_3OO and CD_3OO.

Molecule	State		Calc.[a] $\nu=0$	Ref. 9 $\nu=0$	Ref. 13 $\nu=0$	Expt.[b] $\nu=0$	Expt.[b] $\nu_7=1$
CH_3OO	$\tilde{X}$	A''	1.766	1.716	1.730		
		B''	0.376	0.384	0.379		
		C''	0.330	0.348	0.330		
	$\tilde{A}$	A'	1.606	1.528		1.525	1.526
		B'	0.378	0.391		0.388	0.388
		C'	0.325	0.345		0.326	0.323
CD_3OO	$\tilde{X}$	A''	1.315	1.296	(1.288)[c]		
		B''	0.318	0.332	(0.321)[c]		
		C''	0.284	0.290	(0.284)[c]		
	$\tilde{A}$	A'	1.220	1.182		1.172	1.169
		B'	0.320	0.340		0.329	0.329
		C'	0.281	0.288		0.280	0.280

[a]Calculated with the UB3LYP/aug-cc-pVTZ method.
[b]Fitted parameters for the upper state, where the ground rotational parameters from Ref. 13 were fixed.
[c]Estimated by using observed values of CH_3OO multiplied by ratios of rotational parameters of CD_3OO to CH_3OO calculated quantum chemically.

values of the vibrational modes $\nu_3-\nu_7$ varies as CH_3OO is deuterated. For consistency, we order the vibrational modes of CD_3OO according to the order of CH_3OO so that the vibrational motion is similar for the same mode number. It should be noted that when the $\tilde{X}$ state is excited to the $\tilde{A}$ state, the motion of some vibrational modes varies. In the $\tilde{X}$ state, ν_5 and ν_6 are mixed modes of CH_3 rocking and OO stretching, and ν_7 is mainly the CO stretching mode, whereas in the $\tilde{A}$ state ν_5 involves mainly CH_3 rocking, and ν_6 and ν_7 are mainly COO antisymmetric and symmetric stretching modes, respectively. Predicted displacement vectors for ν_5, ν_6, and ν_7 of CH_3OO and CD_3OO in their $\tilde{X}$ and $\tilde{A}$ states are shown in Fig. 2.

According to quantum-chemical calculations, the O–O bond length of the $\tilde{A}$ state becomes substantially greater than that of the $\tilde{X}$ state. All modes involving OO stretching motion should therefore become active in the $\tilde{A}\leftarrow\tilde{X}$ transition, namely, ν_6 and ν_7 of the $\tilde{A}$ state that are associated with antisymmetric and symmetric COO stretching motions, respectively. The ν_5 mode of CH_3OO is associated mainly with the CH_3 rocking motion, whereas that in CD_3OO is mixed with the symmetric COO stretching (ν_7) mode. Hence, in CD_3OO, the intensity of a transition in ν_5 is increased at the expense of the intensity of one in ν_7. The COO bending (ν_8) mode of CH_3OO and CD_3OO is also expected to be active in the $\tilde{A}\leftarrow\tilde{X}$ transition.

The CH_3 torsional mode (ν_{12}) of CH_3OO and CD_3OO couples readily with other vibrational modes; calculated Franck-Condon factors (to be discussed in Sec. IV E) of the series $N_0^1 12_{\nu''}^{\nu'}$ in which $N=5$, 6, or 7 and $\nu''=\nu'=0,1,2$, decrease by only about 20% for each increase in quantum num-

TABLE II. Comparison of harmonic vibrational frequencies (in cm^{-1}) of CH_3OO and CD_3OO in their $\tilde{X}$ states calculated with the UB3LYP/aug-cc-pVTZ method.

Mode	Vibration	CH_3OO	CD_3OO
ν_1	CH_3 sym. stretch	3150	2340
ν_2	CH_3 total sym. stretch	3050	2180
ν_3	CH_3 deformation	1483	1069
ν_4	CH_3 umbrella	1442	1090
ν_5	CH_3 rock+OO stretch[a]	1217	1197
ν_6	CH_3 rock+OO stretch[b]	1150	991
ν_7	CO stretch[b]	911	831
ν_8	COO bend	490	445
ν_9	CH_3 asym. stretch	3138	2330
ν_{10}	CH_3 asym. deformation	1473	1064
ν_{11}	CH_2 wag	1127	865
ν_{12}	CH_3 torsion	131	104

[a]For CD_3OO, this mode is mainly OO stretch.
[b]For CD_3OO, this mode is mainly mixed with CH_3 rock and CO stretch.

TABLE III. Comparison of harmonic vibrational frequencies (in cm^{-1}) of CH_3OO and CD_3OO in their $\tilde{A}$ states calculated with the UB3LYP/aug-cc-pVTZ method.

Mode	Vibration	CH_3OO	CD_3OO
ν_1	CH_3 sym. stretch	3143	2331
ν_2	CH_3 total sym. stretch	3023	2163
ν_3	CH_3 deformation	1507	1090
ν_4	CH_3 umbrella	1449	1109
ν_5	CH_3 rock[a]	1171	956
ν_6	COO antisym. stretch	1019	1013
ν_7	COO sym. stretch[a]	917	841
ν_8	COO bend	370	343
ν_9	CH_3 asym. stretch	3090	2295
ν_{10}	CH_3 deformation	1466	1062
ν_{11}	CH_3 wag	1166	896
ν_{12}	CH_3 torsion	248	193

[a]These two modes are also mixed; the mixing is more extensive for CD_3OO.

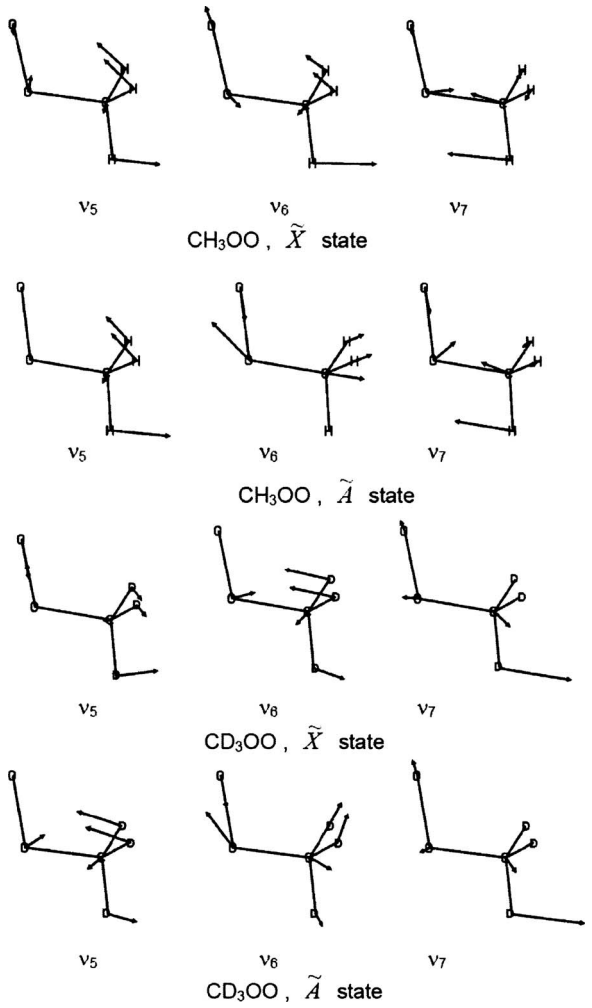

FIG. 2. Vibrational displacement vectors for ν_5, ν_6, and ν_7 modes of CH_3OO and CD_3OO in their $\tilde{A}$ and $\tilde{X}$ states.

ber ν of ν_{12}; the $N_{\nu''}^{\nu'}$ notation, whereby N indicates the vibrational mode, and ν'' and ν' are vibrational quantum numbers of the ground and excited states, respectively, is used throughout the paper. The population of $\nu''=1$ of ν_{12} is ~52% of that of the vibrational ground state for CH_3OO and ~60% for CD_3OO at room temperature; hence the intensities of those hot bands involving these and higher torsional levels are non-negligible. Correspondingly these hot band transitions play a significant role in the spectrum observed at room temperature.

IV. EXPERIMENTAL RESULTS AND DISCUSSION

A. Vibronic bands of CH_3OO (7200–8200 cm^{-1})

1. Nontorsional vibrations

Figure 3 shows the $\tilde{A}\leftarrow\tilde{X}$ electronic spectrum of methyl peroxy (CH_3OO) recorded from 7200 to 8200 cm^{-1} (1.22–1.39 μm). As has been previously reported by Pushkarsky *et al.*,[9] the origin band (indicated as 0_0^0 in Fig. 3) for methyl peroxy is located at 7382.8±0.5 cm^{-1}. In addition to the origin band, Pushkarsky *et al.*[9] also assigned the band at 7488 cm^{-1}, which exhibits similar rotational structure to the origin band, to a transition involving the methyl torsion (ν_{12})

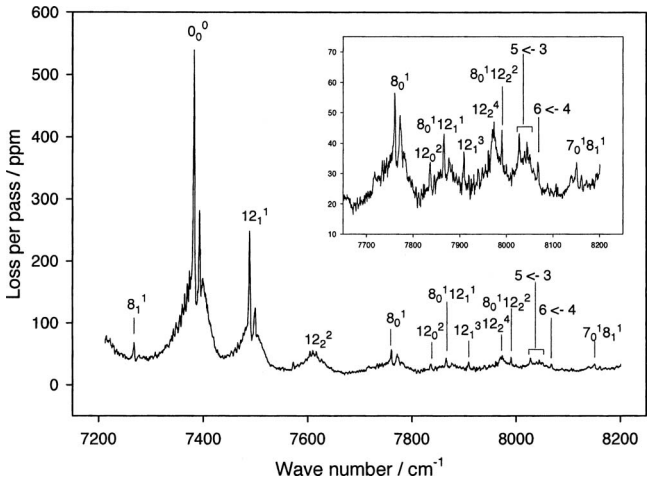

FIG. 3. Experimental spectrum of CH_3OO in the region of 7200–8200 cm^{-1}, digitally smoothed by three points. The region from 7650 to 8200 cm^{-1} has been blown up by a factor of 10 in the inserted box. The notation of the assignments is described in the text.

in the radical. In addition to these previously assigned bands, Fig. 3 includes much more rovibrational structure, some of which exhibits band structure very different from that of the origin.

As has been observed in previous spectroscopic studies of the $\tilde{A}\leftarrow\tilde{X}$ electronic transition of alkyl peroxy radicals,[19,20] one should expect to observe structure due to the COO bend (ν_8 in methyl peroxy) since this vibrational motion involves the terminal oxygen atom in the peroxy radical, where the $\tilde{A}\leftarrow\tilde{X}$ electronic transition is localized. At 7761 cm^{-1}, a fundamental transition in ν_8, which is allowed in a one photon transition since the COO bending mode has a' symmetry, is assigned. This transition is indicated as 8_0^1 in Fig. 3. The assignment is made by referencing the calculated vibrational frequency of ν_8, 370 cm^{-1} in the $\tilde{A}$ state of CH_3OO (Table III), which is in excellent agreement with the experimental observation for 8_0^1 of 378 cm^{-1}. As independent evidence, the similarity in the partially resolved rotational structure (i.e., strong Q-branch character) of this band and the origin also led us to the assignment of both bands to methyl peroxy. It should also be stated here that all bands assigned in Fig. 3 to methyl peroxy were further verified as such by changing the delay time in our experiments, between firing the photolysis and probe lasers, from 100 μs (standard experimental condition for CH_3OO) to 10 ms. By doing this, we observed that all assigned bands in Fig. 3 displayed similar kinetic behavior, and we could, therefore, be confident that they all belonged to the same chemical species.

In addition to the fundamental transition in the COO bend vibration, there is also some hot band structure involving ν_8, similar to that reported for other alkyl peroxy radicals.[20,29] Located just to the red of the origin, a band at 7266 cm^{-1} is assigned to 8_1^1, due to its excellent agreement with the theoretical prediction (see Table IV). Assuming Boltzmann equilibrium at 300 K (and the calculated ν_8 frequency in the $\tilde{X}$ state from Table II), this gives a predicted intensity for 8_1^1 that is approximately 10% that of the origin band, which matches well with the experimental intensity

TABLE IV. Assignments for the observed vibrational bands in the 7200–8600 cm^{-1} region for the $\tilde{A}\leftarrow\tilde{X}$ transition of methyl peroxy (CH_3OO). The experimental shifts from the origin band (0_0^0) are compared with those predicted by theory. The theoretical shifts (see Ref. 30) are calculated between the band maxima for 0_0^0 and the band involved.

Assignment[a]		Observed frequencies (cm^{-1})	Experimental shift (cm^{-1})	Calculated harmonic shift[b,c] (cm^{-1})	Calculated shift[c,d] (cm^{-1})
0_0^0		7383	0		
8_1^1		7266	−117	−120	
12_1^1	$1\leftarrow1$	7488	+105	+117	+101
12_2^2	$2\leftarrow2$	7610	+227	+234	+207
8_0^1		7761	+378	+370	
12_0^2	$2\leftarrow0$	7836	+453	+496	+444
$8_0^1 12_1^1$		7865	+482	+487	
12_1^3	$3\leftarrow1$	7909	+526	+613	+521
12_2^4	$4\leftarrow2$	7972	+589	+730	+601
$8_0^1 12_2^2$		7990	+607	+604	
	$5\leftarrow3$[e]	8027	+644	+847	+675
		8045	+662		
	$6\leftarrow4$	8067	+684	+964	+709
$7_0^1 8_1^1$		8151	+768	+797	
7_0^1		8269.6	+886.8	+917	
$7_0^1 12_1^1$		8375.5[f]	+992.7	+1034	
6_0^1		8376.5[f]	+993.7	+1019	

[a]The transitions are labeled in the Herzberg (left side) as well as the G_6 notation (right side), where it was necessary. See text for more details.
[b]Shifts derived using the quantum chemically calculated harmonic vibrational frequencies in both the ground and excited states from Tables II and III.
[c]For the $\Delta\nu_{12}=0$ torsional transitions, the predicted values in columns 4 and 5 both match relatively well with the experimental value in column 3. For the $\Delta\nu_{12}=2$ torsional transitions, the agreement between the experimental values and the predicted values from column 5 is significantly better than with the predicted values from column 4.
[d]Shifts predicted from theoretical model (Ref. 30), which fits the PES of both the ground and excited states, described by ν_{12}.
[e]Two peaks are observed and ascribed to the $5\leftarrow3$ transition, given that both are closer to the predicted frequency of this band than any others. The $5\leftarrow3$ transition, like other transitions in ν_{12}, is really a convolution of the $5A_2\leftarrow3A_2$ and $5E\leftarrow3E$ transitions, with significant unresolvable K structure in each. However, somewhat larger than most, the theoretical model (Ref. 30) predicts the $5\leftarrow3$ band to be ~25 cm^{-1} wide due to the K-dependent tunneling splitting, which makes it difficult to identify one peak position.
[f]Overlapped; see text.

ratio between the two (~6%). At the blue edge of the spectrum in Fig. 3, there is also a combination band assigned to $8_1^1 7_0^1$, lending further support that 8_1^1 is correctly assigned. The 7_0^1 transition is assigned explicitly in Sec. IV C to a fundamental transition in the coupled CO and OO symmetrically stretching vibrational modes for CH_3OO.

2. Typical torsional sequence bands

Excluding the origin band and the structure due to the COO bending mode (ν_8) assigned above, the remaining spectrum in Fig. 3 is almost exclusively comprised of transitions involving the methyl torsion vibrational mode (ν_{12}).

As mentioned briefly at the beginning of Sec. IV A 1, the band at 7488 cm^{-1} was previously assigned, in a general sense, to a transition in ν_{12} by Pushkarsky *et al.*,[9] but the exact assignment, as far as quantum numbers, was only reported previously by Hunziker and Wendt[8] in a much lower resolution experiment than the ones described in this paper. Concurring with these previous assignments, the peak at 7488 cm^{-1} is assigned to 12_1^1 for several reasons, one of which is that its location (+105 cm^{-1} from the origin) is in good agreement with the predicted value (+117 cm^{-1} from the origin), obtained from the calculated frequencies of ν_{12} in the ground and excited states (see Table IV).

Using the predicted Boltzmann population for $\nu_{12}''=1$ from Sec. III and assuming the same Franck-Condon factor for 12_1^1 and 0_0^0, this hot band should be about half the intensity of the origin band. Not only are the predicted and observed intensities in good agreement, but also the rotational structure of this band matches closely with that of the origin band, further adding confidence that it should be assigned to methyl peroxy. The second member of this sequence band progression is indicated as 12_2^2 in Fig. 3. The intensity difference between 12_1^1 and 12_2^2 is consistent with expectations based upon the above assumptions for 12_1^1. Its distinctly different "rotational" structure requires more explanation and is discussed below in Sec. IV A 3.

In addition to observing the ν_{12} sequence band progression with the origin, we also observe similar sequence bands in combination with the COO bend vibration, giving the $8_0^1 12_1^1$ and $8_0^1 12_2^2$ assignments shown in Fig. 3. These results are also listed in Table IV.

3. Atypical torsional bands

The previous assignments account for about half of the bands in Fig. 3 for methyl peroxy. The remaining assignments are all to additional transitions in the methyl torsion vibrational mode (ν_{12}), which arise from atypical and somewhat unexpected phenomena.

Assignments of these remaining transitions require knowledge about the cut along the methyl torsion vibrational mode of the potential energy surface (PES) for both the $\tilde{X}$ and $\tilde{A}$ states of methyl peroxy. Details of these considerations are described elsewhere,[30] but in general, the calculated PES for the ground state has three degenerate energy minima, where the peroxy OO is staggered with respect to the methyl hydrogens. While the predicted vibrationless and $\nu''_{12}=1$ levels reside well within the wells of this PES, the $\nu''_{12}=2$ level is very close to the top of the energy barrier for methyl rotation, predicted to be about 300 cm^{-1}. This closeness in energy in the ground state PES between the barrier height and two quanta in ν_{12} has several consequences. One consequence is that transitions originating from $\nu''_{12}=2$ will exhibit different "rotational" band structures, as is observed in the case of 12^2_2, from those transitions originating from $\nu''_{12}=0$ or 1 (see also Sec. IV F). This structural difference is mainly caused by the fact that, as the vibrational level nears the barrier top, the tunneling splitting becomes experimentally observable (at our experimental resolution) as the near threefold degeneracy of each methyl rotor level at the bottom of the well splits into a twofold degenerate and a nondegenerate level. Upon rising above the barrier into the free rotor limit, the energy levels instead become doubly degenerate, corresponding to clockwise and counterclockwise rotations. Details of this, as well as a more quantitative explanation of the torsional eigenpairs, appear in an accompanying paper.[30]

A convenient way to consistently label the methyl rotor levels independent of their positions with respect to the barrier height is to invoke the G_6 molecular symmetry group (isomorphic to C_{3v}). The methyl rotor eigenfunctions transform as either A_1, A_2, or E. Near the bottom of the well, the A_1 and A_2 alternately combine with an E to form the nearly threefold degenerate eigenfunctions, which can be labeled by a single torsional quantum number ν_{12}. Well above the barrier, A_1 and A_2 become nearly degenerate and, along with the E eigenfunction, correspond approximately to the doubly degenerate free rotor functions. Eigenvalue and function labels of oA_1, pA_2, and qE, where o, p, and q are even, odd, and all integers, respectively, increasing with the eigenenergy, are therefore the unifying labeling system between levels above and below the barrier. In addition, for levels far below the barrier, we will use the appropriate ν_{12} notation (Herzberg). Note that our labeling of a transition as $5\leftarrow3$ comprises both the $5A_2\leftarrow3A_2$ and the $5E\leftarrow3E$ component transitions, which are not individually resolved in our spectra.

The PES of the $\tilde{A}$ state exhibits a similar phenomenon, albeit the predicted barrier of ~1100 cm^{-1} is much higher. Using the calculated value for ν'_{12} in Table III, one can estimate that we would expect to see an observable tunneling effect near $\nu'_{12}=5$.

The relatively small torsional barriers in both the $\tilde{X}$ and $\tilde{A}$ states have interesting spectral consequences beyond the splitting of the 12^2_2 sequence band due to $\tilde{X}$ state tunneling. While traditional sequence bands $12^{\nu'}_{\nu''}$ ($\nu''_{12}\leqslant2$) have good Franck-Condon factors, the transitions from $\nu''_{12}\geqslant3$, with more free-rotor-like eigenfunctions, to $\nu'_{12}\leqslant4$, with more torsional-like eigenfunctions, will have relatively poor Franck-Condon factors. Concomitantly, transitions from the $\tilde{X}$ state $n=3$ and 4 levels, with free rotor character, will have, correspondingly, better Franck-Condon factors for transitions to $\tilde{A}$ state levels also near the barrier top, e.g., $n=5$ and 6. Using these principles and the quantitative predictions of Ref. 30 as guides, the additional structure in Fig. 3 could now be assigned to "atypical torsional" transitions.

A few features of these "atypical torsional" assignments are worth noting. While tunneling is enough to cause broadening in the band contour of 12^4_2 ($4A_1/E\leftarrow2A_1/E$), in the $5A_2/E\leftarrow3A_2/E$ transition, two clearly resolved peaks are observed in the spectrum (see Fig. 3). Despite this observation, we cannot make definitive assignments of these two peaks to the $A_2\leftarrow A_2$ and $E\leftarrow E$ components, largely because, under our experimental conditions many K levels are populated. Therefore, the K splitting is quite varied and often competitive with the tunneling splitting, with the observed peaks largely resulting from constructive reenforcement between the A_2 and E K-averaged band contours. For the transition $6A_1/E\leftarrow4A_1/E$, we again observe a single sharp peak, whose frequency is listed in Table IV. There is structure to the blue of this peak, which could also be ascribed to the $6\leftarrow4$ transition; however, the signal-to-noise ratio is too poor to make any definitive assignments. This change in peak width from the $5\leftarrow3$ to the $6\leftarrow4$ transition is consistent with calculations,[30] which predict a bandwidth that is approximately two times larger for the $5\leftarrow3$ transition than for $6\leftarrow4$. Additionally, while all of the transitions in the putative $\Delta\nu_{12}=2$ progression are considerably weaker than the origin band, as expected, the intensities of 12^4_2 and $5\leftarrow3$ are larger than, or comparable to, 12^3_1 and 12^2_0 even though the Boltzmann factor decreases as ν''_{12} increases. This increased intensity occurs from better overlap of the corresponding eigenfunctions.

The assignments for the atypical torsional features in Fig. 3 were all based on the calculated transition energies listed in column 5 of Table IV. The agreement between the observed and calculated values is in all cases at least satisfactory.

4. Vibrational analysis

The vibrational and anharmonic coefficients for the methyl torsional vibration (ν_{12}) of the ground $\tilde{X}$ state (ω''_e and $\omega_e x''_e$) and excited $\tilde{A}$ state (ω'_e and $\omega_e x'_e$) were determined by fitting the observed transition frequencies to the standard expansion formula

$$\tilde{\nu}=T_{00}+\omega'_e(\nu'+1/2)-\omega_e x'_e(\nu'+1/2)^2-[\omega'_e/2-\omega_e x'_e/4]-\omega''_e(\nu''+1/2)+\omega_e x''_e(\nu''+1/2)^2+[\omega''_e/2-\omega_e x''_e/4]. \quad (5)$$

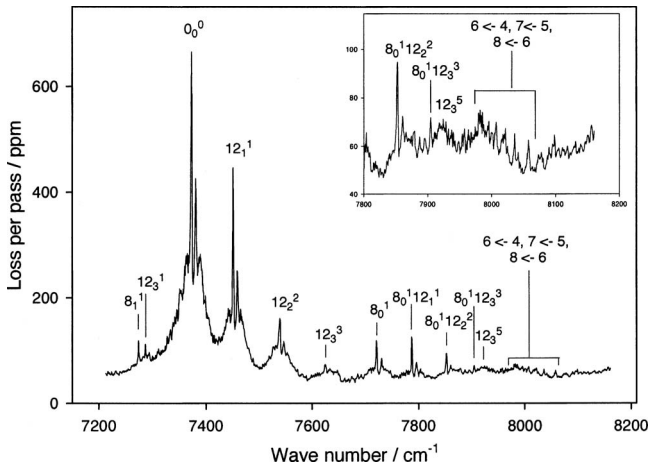

FIG. 4. Experimental spectrum of CD_3OO in the region of 7200–8200 cm^{-1}, digitally smoothed by three points. The region from 7800 to 8200 cm^{-1} has been blown up by a factor of 10 in the inserted box. The notation of the assignments is described in the text.

In the fit, T_{00} was held fixed at the experimentally measured transition origin of 7382.8 cm^{-1}. The fit included only those transitions which originate from a vibrational level bound within the methyl torsional potential, i.e., $\nu''_{12} \leqslant 2$. The following values resulted from the fit: $\omega'_2 = 262.5(47)$ cm^{-1}, $\omega_e x'_e = 11.3(9)$ cm^{-1}, $\omega''_e = 169.7(80)$ cm^{-1}, and $\omega_e x''_e = 18.1(24)$ cm^{-1}, where the uncertainty represents one standard deviation in the fit. The experimental values for the vibrational constants ω'_e and ω''_e are in reasonable agreement with the quantum chemically determined harmonic vibrational frequencies of 248 and 131 cm^{-1} for the excited and ground states, respectively.

B. Vibronic bands of CD_3OO (7200–8200 cm^{-1})

1. Nontorsional vibrations

Figure 4 shows the $\tilde{A} \leftarrow \tilde{X}$ electronic spectrum of deuterated methyl peroxy (CD_3OO) recorded in the 7200–8200 cm^{-1} (1.22–1.39 μm) region. As has been previously reported by Pushkarsky *et al.*,[9] the origin band (indicated as 0_0^0 in Fig. 4) for CD_3OO is located at 7372.6±0.5 cm^{-1}. As was the case for CH_3OO, the electronic spectrum of CD_3OO exhibits much rovibrational structure. Some of these vibrational bands possess band contours similar to 0_0^0 while others are very different.

The spectrum of CD_3OO is again largely comprised of methyl torsion vibrations, with the remaining vibrational structure involving the COO bend vibrational mode (ν_8). As Fig. 4 shows, we have assigned bands at 7721 and 7273 cm^{-1} to 8_0^1 and 8_1^1 of CD_3OO, similar to assignments for CH_3OO. The $8_1^1 7_0^1$ transition that was observed in the spectrum of normal methyl peroxy is missing in the spectrum for the deuterated isotopomer; it is predicted to be 739 cm^{-1} to the blue of the origin band, and therefore, should lie at ~8100 cm^{-1}, which is just to the blue of this spectrally dense region localized around 8000 cm^{-1}. In the zoom of this region in Fig. 4 (see box insert), it is easy to notice some unassigned structure in the region where we expect to see this transition, but the signal-to-noise ratio is too poor to make any definitive assignments.

2. Typical torsional sequence bands

The remaining vibrational structure in the spectrum of CD_3OO is all due to transitions involving the methyl torsion (ν_{12}). Many of these observed transitions in CD_3OO were observed in the spectrum of CH_3OO and assigned in detail in Sec. IV A 2 and IV A 3, and so will only be briefly explained here. Differences between the two species' spectra will be emphasized instead.

Due to the fact that the methyl torsion is the lowest energy vibrational mode in CD_3OO, and that it lies even lower in energy than in CH_3OO (predicted only 104 cm^{-1} above $\nu''=0$ in CD_3OO as opposed to 131 cm^{-1} in CH_3OO, as listed in Table II), we would again expect to observe sequence structure. Hence Fig. 4 and Table V show the assignments 12_1^1, 12_2^2, and 12_3^3. Due to the decrease in energy of the vibrational mode upon deuteration, we observe a third member of this sequence band (12_3^3), which was not observed in CH_3OO. The intensity ratios of the various members of the sequence band in ν_{12} with respect to the origin are in agreement with what is predicted by the Boltzmann factor assuming similar Franck-Condon factors.

The structural similarity between the origin and 12_1^1 bands that was observed in normal methyl peroxy is also observed for CD_3OO, i.e., both 0_0^0 and 12_1^1 exhibit very sharp partially resolved rotational structure. In CH_3OO, the 12_2^2 band had a very different band structure from 0_0^0 and 12_1^1 because of tunneling, due to the closeness of the $\nu''_{12}=2$ vibrational level to the top of the barrier. Tunneling effects also occur in CD_3OO, since deuteration does not affect the potential energy surface, but only the energy level spacing therein. In CD_3OO, the 12_2^2 band is slightly broader than 12_1^1, and the 12_3^3 band exhibits an even broader band contour with less noticeable sharp structure because $\nu''_{12}=3$ is near the barrier to free methyl rotation.

In addition to observing the sequence band progression in ν_{12} to the blue of the origin, we also observe combinations of this progression with the COO bend vibration in the $\tilde{A}$ state. This leads to the $8_0^1 12_1^1$, $8_0^1 12_2^2$, and $8_0^1 12_3^3$ assignments in Fig. 4, which as Table V shows are in good agreement with the prediction from calculations.

3. Atypical torsional bands

Similar to methyl peroxy, the remaining assignments made in the electronic spectrum of CD_3OO (Fig. 4) are all due to somewhat atypical or unexpected transitions in the methyl torsion due to thermal population of levels near or above the barrier height.

There are many transitions in CD_3OO similar to those observed in CH_3OO. The same sequence band progression of $\Delta\nu_{12}=2$ transitions observed in the normal methyl peroxy is also observed in deuterated methyl peroxy. Whereas this progression started with the 12_0^2 transition in CH_3OO, the

TABLE V. Assignments for the observed vibrational bands in the 7200–8600 cm^{-1} region for the $\tilde{A}\leftarrow\tilde{X}$ transition of deuterated methyl peroxy (CD_3OO). The experimental shifts from the origin band (0_0^0) are compared with those predicted by theory. The theoretical shifts (see Ref. 30) are calculated between the band maxima for 0_0^0 and the band involved.

Assignment[a]		Observed frequencies (cm^{-1})	Experimental shift (cm^{-1})	Calculated harmonic shift[b,c] (cm^{-1})	Calculated shift[c,d] (cm^{-1})
0_0^0		7373	0		
12_3^1	$1\leftarrow3$	7286	−87	−119	−95
8_1^1		7273	−100	−102	
12_1^1	$1\leftarrow1$	7451	+78	+89	+76
12_2^2	$2\leftarrow2$	7538	+165	+178	+159
12_3^3	$3\leftarrow3$	7624	+251	+267	+244
8_0^1		7721	+348	+343	
$8_0^1 12_1^1$		7787	+414	+432	
$8_0^1 12_2^2$		7852	+479	+521	
$8_0^1 12_3^3$		7904	+531	+610	
12_3^5	$5\leftarrow3$	7923	+550	+653	+546
	$6\leftarrow4$[e]	7982	+609	+742	+615
		7995	+622		
	$7\leftarrow5$[e]	8006	+633	+831	+651
		8018	+645		
	$8\leftarrow6$[e]	8035	+662	+920	+660
		8058	+685		
7_0^1		8196.3	+823.7	+841	
$6_0^1 12_3^1$		~8250	+877.4	+894	
$7_0^1 12_1^1$		8275.0	+902.4	+930	
5_0^1		8327.0	+954.4	+956	
6_0^1		8343.5	+970.9	+1013	
$7_0^1 12_2^2$		~8354	+981.6	+1019	
$5_0^1 12_1^1$		8403.0	+1030.4	+1045	
$6_0^1 12_1^1$		8420.0	+1047.4	+1102	
$5_0^1 12_2^2$		8490.5	+1117.9	+1134	
$6_0^1 12_2^2$		8510.0	+1137.4	+1191	

[a]The transitions are labeled in the Herzberg (left side) as well as the G_6 notation (right side), where it was necessary. See text for more details.
[b]Shifts derived using the quantum chemically calculated harmonic vibrational frequencies in both the ground and excited states from Tables II and III.
[c]For the $\Delta\nu_{12}=0$ torsional transitions, the predicted values in columns 4 and 5 both match relatively well with the experimental value in column 3. For the $\Delta\nu_{12}=2$ torsional transitions, the agreement between the experimental values and the predicted values from column 5 is significantly better than with the predicted values from column 4.
[d]Shifts predicted from theoretical model, (Ref. 30), which fits the PES of both the ground and excited states, described by ν_{12}.
[e]While experimentally observed peaks have been ascribed to the $6\leftarrow4$, $7\leftarrow5$, and $8\leftarrow6$ transitions in the table, the theoretical model (Ref. 30) predicts that the broad band contours of each of these will overlap due to the *K*-dependent tunneling splitting, making it difficult to assign a peak or peaks in this range to a particular transition. Therefore, we instead assign all six peaks to all three predicted transitions $6\leftarrow4$, $7\leftarrow5$, and $8\leftarrow6$, as shown in Fig. 3.

first member observed in CD_3OO is 12_3^5. Because of the more abundant structure in the COO bend region of the spectrum (7700–7900 cm^{-1}), the earlier members of this sequence band progression are not observed/resolved for the deuterated isotopomer, due to their overlap with other, already assigned, structure in the spectrum. For example, 12_0^2 is predicted to be 351 cm^{-1} to the blue of the origin band in CD_3OO,[30] which directly coincides with the rotational contour of the 8_0^1 band. This is also the case for the 12_1^3 and 12_2^4 transitions, which were observed in CH_3OO, but overlap with $8_0^1 12_1^1$ and $8_0^1 12_2^2$, respectively, in CD_3OO. Differing from CH_3OO, the 12_3^5 transition is still assigned in the $12_{\nu''}^{\nu'}$ notation, as $\nu''_{12}\geqslant4$ levels lie above the barrier for CD_3OO.

The remaining members observed in this $\Delta\nu_{12}=2$ progression all originate from $\nu''_{12}\geqslant4$ levels and are better described by the G_6 labels. Based on the calculated transition energies (see column 5 of Table V), bands from ~7980 to 8060 cm^{-1} have been assigned to the $6\leftarrow4$, $7\leftarrow5$, and $8\leftarrow6$ transitions collectively, since their predicted[30] band contours, broadened both because of tunneling and *K* structure, largely overlap. The $7\leftarrow5$ and $8\leftarrow6$ transitions in CD_3OO are all missing from the spectrum of CH_3OO, most likely due to the lower Boltzmann population of the $\nu''_{12}=5$ and 6 levels in CH_3OO.

In CD_3OO, the peak at 7286 cm^{-1} (−87 cm^{-1} from the origin) is assigned to the 12_3^1 transition based on its relatively

good agreement with the calculated shifts of this band, both by the quantum chemically calculated frequencies of ν_{12} in the ground and excited states (see column 4 of Table V) and by the more accurate theoretical model[30] (see column 5 of Table V). The corresponding transition in CH_3OO is not observed because its band center is predicted to be -94 cm^{-1} from the origin, which yields potential overlap of this transition with 8_1^1. In addition, 12_3^1 in CH_3OO suffers considerably more from the tunneling effect than it does in CD_3OO, since it originates from a vibrational level that is close to the barrier. Hence its contour is likewise predicted[30] to be roughly two times broader than in CD_3OO.

Additional structure with less intensity is predicted[30] in the region above 8060 cm^{-1} and is also experimentally observed in the spectra. However, an exact line by line assignment is not straightforward here due to the high density of lines predicted theoretically.

4. Vibrational analysis

A similar vibrational analysis for deuterated methyl peroxy using transitions originating from levels with $\nu_{12}''\leqslant 3$ corresponding to bound CD_3 torsional levels (see Table V) and a value of 7372.6 cm^{-1} for the experimental transition origin resulted in $\omega_e'=196.4(36)$ cm^{-1}, $\omega_e x_e'=5.3(5)$ cm^{-1}, $\omega_e''=121.4(49)$ cm^{-1}, and $\omega_e x_e''=7.6(10)$ cm^{-1}, in close agreement with the quantum-chemical calculations of 193 cm^{-1} and 104 cm^{-1} for ω_e' and ω_e'', respectively.

C. Vibronic bands of CH_3OO (8170–8450 cm^{-1})

Trace A of Fig. 5 presents the spectrum of CH_3OO in the region of 8170–8450 cm^{-1} (1.18–1.22 μm). Although the mirror set used covers the range of 7700–8900 cm^{-1}, the region above 8459 cm^{-1} was subject to interference from absorption of the parent molecule acetone. In this spectral region, two bands with a rotational structure similar to that of the origin band were observed. The band near 8270 cm^{-1} is separated from the reported origin[9] at 7382.8 cm^{-1} by $\sim$887 cm^{-1}; it is readily assigned as the 7_0^1 band of the $\tilde{A}\leftarrow\tilde{X}$ transition based on $\nu_7'=917$ cm^{-1} predicted with quantum-chemical calculations; predicted vibrational frequencies of other vibrational modes of the $\tilde{A}$ state, which would have allowed fundamental transitions, deviate from 887 cm^{-1} by more than 15% and are thus unlikely to be assigned to this band. Although the ν_7 mode is associated mainly with the CO stretching motion in the ground electronic state, it becomes a mixed mode coupled with mainly symmetric CO and OO stretching motions in the $\tilde{A}$ state. By comparison of the geometries of the $\tilde{A}$ and $\tilde{X}$ states, we expect modes associated with OO stretching to be most active because the length of the O–O bond increases from 1.317 to 1.385 Å upon excitation to the $\tilde{A}$ state.

The rotational parameters of CH_3OO in its $\tilde{X}$ state have been determined with microwave spectroscopy; the preliminary results yield $A_0''=1.730$, $B_0''=0.379$, and $C_0''=0.330$ cm^{-1}.[13] We fixed these values for the ground state and varied values of A', B', C', and $\nu(7_0^1)$ for the best fit of the observed spectrum. The simulated spectrum of the 7_0^1 band, shown in Fig. 5(B), is similar to experimental observation shown in Fig. 5(A). Optimization of the fit yielded $\nu(7_0^1)=8269.6$ cm^{-1}, $A'=1.526$ cm^{-1}, $B'=0.388$ cm^{-1}, and $C'=0.323$ cm^{-1}, as listed in Table I. The band origin deviates from the origin of the $\tilde{A}\leftarrow\tilde{X}$ transition at 7382.8 cm^{-1} (Ref. 9) by 886.8 cm^{-1}, near a value of $\sim$890 cm^{-1} derived previously from low-resolution absorption spectra,[8] and a value of 898 cm^{-1} derived from IR+VUV PFD experiments.[12]

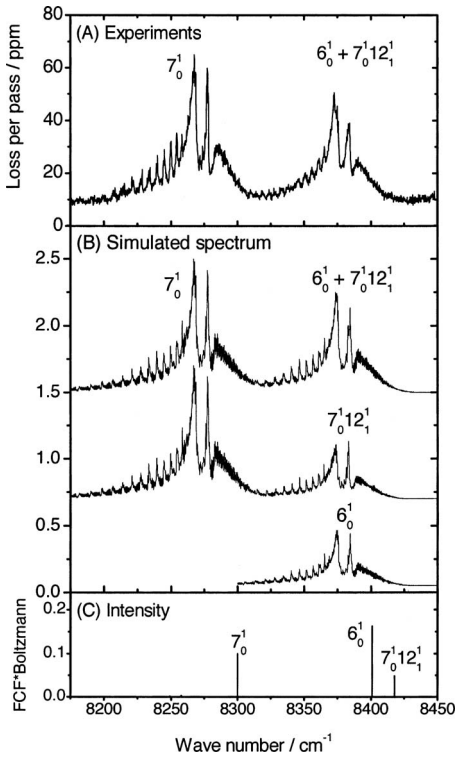

FIG. 5. (A) Experimental spectrum of CH_3OO in the region of 8170–8450 cm^{-1}. (B) Simulated spectrum using experimental rotational parameters of the $\tilde{X}$ state (Ref. 13) and fitted parameters of the $\tilde{A}$ state; see text for details. (C) Calculated Franck-Condon factors multiplied by Boltzmann factors of the lower state.

Similar fitting procedures were performed for the band near 8375 cm^{-1}, about 993 cm^{-1} above the origin of the $\tilde{A}\leftarrow\tilde{X}$ transition. This band was assigned as the hot combination band involving 12_1^1, which has been assigned in Sec. IV A 2. For the $\nu_{12}''=1$ state the experimental rotational parameters are unreported. Therefore, we derived these $\tilde{X}$ state parameters for our simulation by determining the ratio between the calculated (UB3LYP/aug-cc-pVTZ) and experimental (A'', B'', and C'' from Ref. 13, as listed in Table I) values for $\nu''=0$ and applying it to the calculated values for $\nu_{12}''=1$. We employed similar procedures to simulate the spectrum with the parameters of the lower state ($\nu_{12}=1$ of the $\tilde{X}$ state) held fixed at the derived values. The simulated spectrum based on the optimized upper-state parameters is shown in the middle trace of Fig. 5(B) for comparison. Values of $\nu(7_0^1 12_1^1)=8375.5$ cm^{-1}, $A'=1.526$ cm^{-1}, $B'=0.386$ cm^{-1}, and $C'=0.322$ cm^{-1} were derived, similar to those of the 7_0^1 band. The band origin deviates from the origin of the $\tilde{A}\leftarrow\tilde{X}$ transition at 7382.8 cm^{-1} by 992.7 cm^{-1},

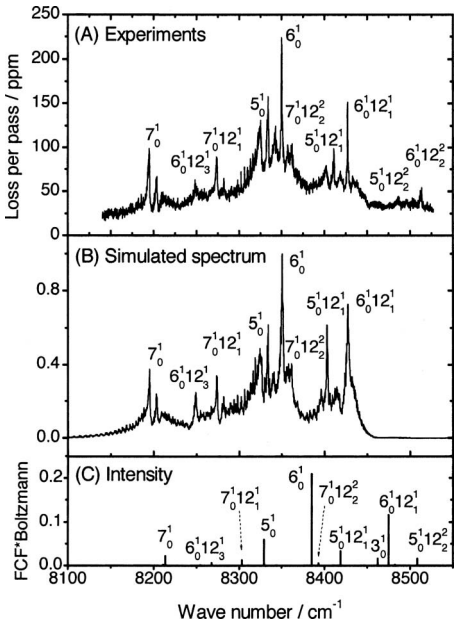

FIG. 6. (A) Experimental spectrum of CD_3OO in the region of 8140–8530 cm^{-1}. (B) Simulated spectrum using experimental rotational parameters of the $\tilde{X}$ state (Ref. 13) and fitted parameters of the $\tilde{A}$ state; see text for details. (C) Calculated Franck-Condon factors multiplied by Boltzmann factors of the lower state.

105.9 cm^{-1} greater than that of the 7_0^1 band. The value of 105.9 cm^{-1} is nearly identical to the separation (105 cm^{-1}, Table IV) of the 12_1^1 band from the origin.

On closer examination, the experimental contour width and the intensity for this band near 8375 cm^{-1} are greater than the simulation on the $7_0^1 12_1^1$ band, indicating the possibility that an additional band is overlapped with this band. As discussed in Sec. III, the ν_6 mode for CH_3OO in its $\tilde{A}$ state is associated mainly with antisymmetric CO and OO stretching motions; hence its activity in the $\tilde{A}\leftarrow\tilde{X}$ transition is also expected. Quantum-chemical calculations predict ν_6 =1019 cm^{-1} for CH_3OO; after scaling based on the ratio (886.8/917) of observed to calculated frequencies of ν_7, ν_6 becomes 985 cm^{-1}, close to the observed band located 993 cm^{-1} from the origin. We simulated the 6_0^1 band, as shown in the lowest trace of Fig. 5(B), and combined it with the simulated contour of the $7_0^1 12_1^1$ band (middle trace) to yield the upper trace in Fig. 5(B), which is in better agreement with the experimental observation. Because of this severe overlap, the accuracies of the frequencies of these two bands are approximately ±1.5 cm^{-1}. A band was observed in IR+VUV PFD experiments 1002 cm^{-1} above the origin and assigned to 6_0^1, close to our value.[12]

D. Vibronic bands of CD_3OO (8140–8530 cm^{-1})

Trace A of Fig. 6 presents the CD_3OO spectrum taken in the region of 8140–8530 cm^{-1} (1.17–1.23 μm). In this spectral region, more bands were observed for CD_3OO than for CH_3OO. The band at 8196.3 cm^{-1} is separated from the reported origin (7372.6 cm^{-1}) by 823.7 cm^{-1};[9] it is readily assigned to the 7_0^1 band of CD_3OO in its $\tilde{A}\leftarrow\tilde{X}$ transition based on ν_7'=841 cm^{-1} predicted with UB3LYP/aug-cc-pVTZ calculations; predicted vibrational frequencies of other vibrational modes of CD_3OO in its $\tilde{A}$ state, for which fundamental transitions would be allowed, all deviate by more than 15% from 823 cm^{-1}. According to calculations, although this ν_7 mode in CH_3OO is described mainly as the COO symmetric stretching motion, it becomes coupled with the CH_3 rocking mode in CD_3OO. The experimental observation of a large deuterium isotopic shift, from 886.8 to 823.7 cm^{-1}, agrees with the predicted mixing.

The ground state rotational parameters for the ν''=0 state of CD_3OO have been estimated by multiplying quantum chemically calculated ratios of these parameters for CD_3OO/CH_3OO by the experimental values of CH_3OO (Ref. 13), as listed in Table I. We then varied values of $\nu(7_0^1)$, A', B', and C' to obtain the best fit of the observed spectrum. The simulated spectrum of the 7_0^1 band, shown in trace B of Fig. 6, is similar to the experimental observation shown in trace A. Optimization of the fit yielded $\nu(7_0^1)$=8196.3 cm^{-1}, A'=1.169, B'=0.329, and C'=0.280 cm^{-1}, as listed in Table I.

Similar fitting procedures were performed for the band near 8275 cm^{-1}, about 902 cm^{-1} above the origin of the $\tilde{A}\leftarrow\tilde{X}$ transition. This band is tentatively assigned to the hot band originating from ν_{12}''=1. We follow the similar procedure (see above) to estimate parameters of the ν_{12}''=1 state of CD_3OO using the ratios of the calculated (UB3LYP/aug-cc-pVTZ calculations) and experimental (Endo's constants[13] A'', B'', and C'', as listed in Table I) values for ν''=0 of CH_3OO and applying them to the calculated ones for ν_{12}''=1 of CD_3OO. The simulated spectrum, using the parameters of the lower state (ν_{12}''=1) unaltered and optimized parameters for the upper state, is shown in trace B of Fig. 6 for comparison. Values $\nu(7_0^1 12_1^1)$=8275.0 cm^{-1}, A'=1.169, B' =0.329, and C'=0.280 cm^{-1} were derived, whereby the rotational parameters are in quantitative agreement with the ones obtained from the 7_0^1 simulation (see Table I). The band origin deviates from the transition origin at 7372.6 cm^{-1} by 902.4 cm^{-1}, 78.7 cm^{-1} greater than that of the 7_0^1 band. This is nearly identical to the observed separation (78 cm^{-1}, Table V) of the 12_1^1 band from the origin of CD_3OO. A possibility of this band to be assigned to 6_0^1, as in the case of CH_3OO, can be positively excluded because quantum-chemical calculations predict a small deuterium shift for this mode, with ν_6=1013 cm^{-1} for CD_3OO. Although the ν_{11} mode of CD_3OO is predicted to be 896 cm^{-1} from the origin, it is symmetry forbidden. The next member of the series, $7_0^1 12_2^2$, is overlapped with the 6_0^1 band; its band origin lies near 8354 cm^{-1}.

Two bands in the 8300–8370 cm^{-1} region have the largest intensities. Spectral fittings according to a similar method yielded $\nu(5_0^1)$=8327.0 cm^{-1} and $\nu(6_0^1)$=8343.5 cm^{-1}, both with A'=1.169, B'=0.329, and C'=0.280 cm^{-1}. Their separations of 954.4 and 970.9 cm^{-1} from the origin are nearest to the vibrational frequencies 956 and 1013 cm^{-1} predicted with the UB3LYP/aug-cc-pVTZ method for ν_5 and ν_6, respectively (see Table III). The order for the frequencies of ν_5 and ν_6 of CD_3OO is reversed from that for CH_3OO because ν_5 is associated mainly with CH_3-rocking motion whereas ν_6

is mainly associated with COO antisymmetric stretching motion; the former has a much greater isotopic shift.

Similarly to the assignment of $7_0^1 12_1^1$, the next two bands are readily assigned to $5_0^1 12_1^1$ and $6_0^1 12_1^1$ transitions, with $\nu(5_0^1 12_1^1)=8403.0\ \mathrm{cm}^{-1}$ and $\nu(6_0^1 12_1^1)=8420.0\ \mathrm{cm}^{-1}$, respectively; they are 1030.4 and 1047.4 cm^{-1} above the origin. The separations of these bands from the corresponding 5_0^1 and 6_0^1 bands are 76.0 and 76.5 cm^{-1}, respectively. Similarly, two weak bands on the high-energy side might be assigned to $5_0^1 12_2^2$ and $6_0^1 12_2^2$ transitions, with $\nu(5_0^1 12_2^2)=8490.5\ \mathrm{cm}^{-1}$ and $\nu(6_0^1 12_2^2)=8510.0\ \mathrm{cm}^{-1}$, respectively. A weak band lying near 8250 cm^{-1} between bands 7_0^1 and $7_0^1 12_1^1$ might be assigned to the $6_0^1 12_3^1$ transition. The observed separation of this weak feature from the 6_0^1 band, $-93.5\ \mathrm{cm}^{-1}$, is close to the separation of $-87\ \mathrm{cm}^{-1}$ for the 12_3^1 band from the origin. Fu *et al.* observed bands at 834, 899, 963, 986, and 1056 cm^{-1} above the origin from the IR+vuv PFD experiments and assigned these bands to 7_0^1, 5_0^1, 6_0^1, 3_0^1, and 4_0^1, respectively, by comparison with quantum-chemical calculations.[12] The assignments 6_0^1 and 7_0^1 are in essential agreement with ours, while considerable discrepancy exists for 5_0^1. We think that our assignments are more reliable because of greater resolution and the consideration of Franck-Condon factors.

E. Calculations of Franck-Condon factors

To explain why more vibronic bands are observed for CD_3OO than for CH_3OO, we calculated multidimensional Franck-Condon factors for the $\tilde{A}\leftarrow\tilde{X}$ transitions of CH_3OO and CD_3OO using a program written by Borrelli and Peluso.[31] The equilibrium geometries, normal mode coordinates, and vibrational frequencies of the $\tilde{A}$ and $\tilde{X}$ states, calculated with the UB3LYP/aug-cc-pVTZ method, were employed. Calculated Franck-Condon factors for the $\tilde{A}\leftarrow\tilde{X}$ transitions of CH_3OO and CD_3OO multiplied by the Boltzmann factors at 300 K for each vibrational level in their $\tilde{X}$ states are shown in trace C of Figs. 5 and 6, respectively. For CH_3OO, bands 7_0^1, 6_0^1, and $7_0^1 12_1^1$ are active in the spectral region of 8200–8500 cm^{-1}; the transition involving ν_6 is predicted to be more intense than those involving ν_7. In contrast, 7_0^1 is observed to be the most intense, and the 6_0^1 band might be overlapped with the $7_0^1 12_1^1$ band and has slightly smaller intensity. It is unclear why the predicted intensity of the 6_0^1 band is greater than experimental observation. One possibility is that the actual ν_6 mode in the $\tilde{A}$ state of CH_3OO contains more CO stretching and less OO stretching motion than quantum-chemical calculations predict, hence it has smaller intensity than that predicted theoretically.

For CD_3OO, the 6_0^1 band is predicted to be the most intense, and transitions involving ν_5 become more intense than those involving ν_7. The observed spectral pattern of CD_3OO fits satisfactorily with the predicted intensity distribution, as shown in trace C of Fig. 6; compared with the spectrum of CH_3OO, the intensity of ν_5 is increased at the expense of the intensity of ν_7.

Franck-Condon factors using the same program were also calculated for CH_3OO and CD_3OO in the range of 7200–8200 cm^{-1}. Whereas they nicely predict the positions and relative intensities for the bands involving ν_8 and typical methyl torsion, they are of lower quality for the atypical methyl torsional bands.

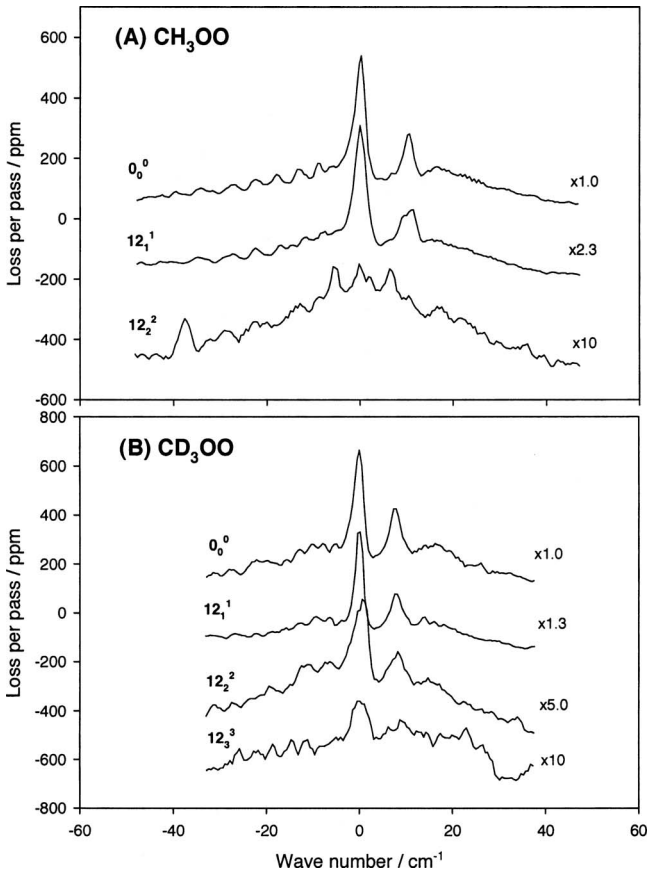

FIG. 7. Comparison between experimental spectra of the 0_0^0 band and members of the sequence band progression in ν_{12} for (A) CH_3OO and (B) CD_3OO. The bands have been centered at 0 to facilitate a comparison of the overall band contours. The intensities of the sequence bands have been multiplied by the factors indicated on each trace to facilitate better comparisons. These traces have also been manually offset (in the y direction) for visualization purposes.

F. Tunneling splitting

As described in Sec. IV A 3, the 12_2^2 transition for methyl peroxy shows a different band structure from that of the origin and 12_1^1 transitions, because the $\nu''_{12}=2$ vibrational level lies sufficiently close to the methyl torsional potential barrier to result in observable tunneling effects. In deuterated methyl peroxy the same phenomenon arises for the 12_3^3 transition, involving one more vibrational quantum because of the lower CD_3 torsional frequency. Figure 7 shows a comparison of the experimentally observed contours of the origin and sequence bands in ν_{12} for both CH_3OO and CD_3OO.

In looking at Fig. 7(A), it is easy to see the similarities in band contour between the 0_0^0 and 12_1^1 for CH_3OO. If a quite low torsional barrier in the $\tilde{X}$ state did not exist, one would expect a very similar band structure for 12_2^2 as well. However, the observed 12_2^2 band contour is very different. Instead of the band being clearly defined by two strong Q-branch peaks, one with approximately two to three times more intensity than the other, the 12_2^2 band is comprised of three comparably intense peaks in the band center and one peak of

lower intensity redshifted from the others by about 40 cm^{-1}. These multiple peaks result from a *K*-dependent splitting of the *A* and *E* energy levels in the $\tilde{X}$ state, giving multiple distinct maxima for the 12_2^2 band when the individual transitions are convoluted. In the 0_0^0 and 12_1^1 bands, the corresponding *A* and *E* energy levels are nearly degenerate in the ground state since they are located within the well of the PES, and an energy splitting is not resolvable given the conditions of our experiment. This very different band contour in 12_2^2 is explained by the $2E\leftarrow 2E$ and $2A_1\leftarrow 2A_1$ transitions, which are no longer degenerate. Rather they suffer a *K*-dependent shift, with the *E* transition suffering a *K*-dependent splitting. The resolution of our experiment limits our ability to extract precise tunneling parameters, but we can estimate from Fig. 7(A) that the splittings present are in the range of 5–20 cm^{-1}. We attribute these observed splittings in the spectrum entirely to tunneling effects in the $\tilde{X}$ state, as the corresponding $\tilde{A}$ level should have negligible splittings since it lies well below the barrier height.

Likewise, in looking at Fig. 7(B), it is easy to see the degradation of the distinct *Q*-branch structure, observed in the 0_0^0 band of CD_3OO, in the higher members of the sequence band progression in ν_{12}. As mentioned above, the 12_3^3 transition in CD_3OO exhibits a similar tunneling effect as the 12_2^2 in CH_3OO, and hence shows the most discrepancy in band structure with the origin. For the 12_3^3 transition in CD_3OO, there is even less "fingerprint" structure resolved than for 12_2^2 in CH_3OO, making precise evaluation of the tunneling parameters impossible from these data. However, clearly the splittings are comparable in the $\nu_{12}''=2$ level in CH_3OO and the $\nu_{12}''=3$ level in CD_3OO, consistent with the theoretical predictions that these levels lie near the $\tilde{X}$ state barrier top.

V. CONCLUSION

We have recorded in the region of 1.18–1.40 μm several rovibronic bands of normal and deuterated methyl peroxy in their $\tilde{A}\leftarrow\tilde{X}$ transitions with the cavity ringdown technique. For CH_3OO, both the COO symmetric stretching (ν_7) and COO bending (ν_8) vibrations in the $\tilde{A}$ state were observed at 887 and 378 cm^{-1}, respectively; the COO antisymmetric stretching mode ($\nu_6\cong 994$ cm^{-1}) might be overlapped with the $7_0^1 12_1^1$ band. For CD_3OO, in addition to ν_7 and ν_8 at 824 and 348 cm^{-1}, two additional $\tilde{A}$ state vibrations were also observed, namely, ν_5 (954 cm^{-1}) and ν_6 (971 cm^{-1}). These experimental results are all in good agreement with quantum-chemical predictions using UB3LYP/aug-cc-pVTZ, and the enhanced activity of the ν_5 mode in CD_3OO is rationalized by mode mixing and is supported by calculations of multidimensional Franck-Condon factors. There is also considerable vibrational structure observed which is due to transitions in the methyl torsional mode (ν_{12}). This structure can be conveniently divided into the "typical" sequence bands and "atypical" transitions in this mode, which are due to the location of the vibrational energy levels with respect to the relatively low, but quite different, energy barriers in the $\tilde{X}$ and $\tilde{A}$ states. Because of the closeness in energy of $\nu_{12}''=2$ in CH_3OO and $\nu_{12}''=3$ in CD_3OO with the torsional barrier height in the $\tilde{X}$ state, the 12_2^2 transition in CH_3OO and 12_3^3 transition in CD_3OO showed significantly different structures than the origin bands.

ACKNOWLEDGMENTS

The authors thank R. Borrelli and A. Peluso for providing a program for the multidimensional Franck-Condon calculations, C. Western for providing the PGopher spectral simulation program, Y. Endo for providing results from their microwave studies of CH_3OO prior to publication, the National Center for High-Performance Computing of Taiwan for computer facilities, and the National Science Council of Taiwan (Grant No. NSC95-2119-M-009-032) and the Ministry of Education, Taiwan (ATU project) for support. They wish to acknowledge the financial support of this work by the Chemical Sciences, Geosciences and Biosciences Division, Office of Basic Energy Sciences, Office of Science, U.S. Department of Energy, via Grant No. DE-FG02-01ER14172. One of the authors (P.R.) thanks the Swiss National Science Foundation for a post-doctoral fellowship.

[1] G. Salisbury, A. R. Rickard, P. S. Monks *et al.*, J. Geophys. Res., [Atmos.] **106**, 12669 (2001) and references therein.
[2] G. S. Tyndall, R. A. Cox, C. Granier, R. Lesclaux, G. K. Moortgat, M. J. Pilling, A. R. Ravishankara, and T. J. Wallington, J. Geophys. Res., [Atmos.] **106**, 12157 (2001) and references therein.
[3] S. Wang, D. L. Miller, N. P. Cernansky, H. J. Curran, W. J. Pitz, and C. K. Westbrook, Combust. Flame **118**, 415 (1999) and references therein.
[4] P. S. Stevens, J. H. Mather, W. H. Brune *et al.*, J. Geophys. Res., [Atmos.] **102**, 6379 (1997).
[5] P. Ase, W. Bock, and A. Snelson, J. Phys. Chem. **90**, 2099 (1986).
[6] S. Nandi, S. J. Blanksby, X. Zhang, M. R. Nimlos, D. C. Dayton, and G. B. Ellison, J. Phys. Chem. A **106**, 7547 (2002).
[7] J. K. Thomas, J. Phys. Chem. **71**, 1919 (1967).
[8] H. E. Hunziker and H. R. Wendt, J. Chem. Phys. **64**, 3488 (1976).
[9] M. B. Pushkarsky, S. J. Zalyubovsky, and T. A. Miller, J. Chem. Phys. **112**, 10695 (2000).
[10] D. B. Atkinson and J. L. Spillman, J. Phys. Chem. A **106**, 8891 (2002).
[11] S. J. Blanksby, T. M. Ramond, G. E. Davico, M. R. Nimlos, S. Kato, V. M. Bierbaum, W. C. Lineberger, G. B. Ellison, and M. Okumura, J. Am. Chem. Soc. **123**, 9585 (2001).
[12] H. B. Fu, Y. J. Hu, and E. R. Bernstein, J. Chem. Phys. **125**, 014310 (2006).
[13] Y. Endo (private communication); K. Katoh, Ph.D. thesis, University of Tokyo, 2007.
[14] R. A. Bair and W. A. Goddard, J. Am. Chem. Soc. **104**, 2719 (1982).
[15] B. H. Besler, M. D. Sevilla, and P. MacNeille, J. Phys. Chem. **90**, 6446 (1986).
[16] J. A. Jafri and D. H. Phillips, J. Am. Chem. Soc. **112**, 2586 (1990).
[17] J. L. Weisman and M. Head-Gordon, J. Am. Chem. Soc. **123**, 11686 (2001).
[18] K. W. Busch and M. A. Busch, *Cavity-Ringdown Spectroscopy—An Ultratrace-Absorption Measurement Technique* (American Chemical Society, Washington, DC, 1999).
[19] B. G. Glover and T. A. Miller, J. Phys. Chem. A **109**, 11191 (2005).
[20] P. Rupper, E. N. Sharp, G. Tarczay, and T. A. Miller, J. Phys. Chem. A **111**, 832 (2007).
[21] L. S. Rothman, C. P. Rinsland, A. Goldman *et al.*, J. Quant. Spectrosc. Radiat. Transf. **60**, 665 (1998).
[22] C.-Y. Chung, J. F. Ogilvie, and Y.-P. Lee, J. Phys. Chem. A **109**, 7854 (2005).
[23] A. D. Becke, J. Chem. Phys. **98**, 5648 (1993).
[24] C. Lee, W. Yang, and R. G. Parr, Phys. Rev. B **37**, 785 (1988).
[25] T. H. Dunning, Jr., J. Chem. Phys. **90**, 1007 (1989).

[26] D. E. Woon and T. H. Dunning, Jr., J. Chem. Phys. **98**, 1358 (1993).
[27] M. J. Frisch, G. W. Trucks, H. B. Schlegel *et al.*, GAUSSIAN 03, Revision A.1, Gaussian, Inc., Pittsburgh, PA, 2003.
[28] G. Herzberg, *Infrared and Raman Spectra of Polyatomic Molecules*, Molecular Spectra and Molecular Structure Vol. II (Krieger, Malabar, 1991).
[29] S. J. Zalyubovsky, B. G. Glover, and T. A. Miller, J. Phys. Chem. A **107**, 7704 (2003).
[30] G. M. P. Just, A. B. McCoy, and T. A. Miller, J. Chem. Phys. **127**, 044310 (2007), preceding paper.
[31] R. Borrelli and A. Peluso, J. Chem. Phys. **119**, 8437 (2003).